

UCSF

UC San Francisco Previously Published Works

Title

Human Facial Shape and Size Heritability and Genetic Correlations

Permalink

<https://escholarship.org/uc/item/5m21v69k>

Journal

Genetics, 205(2)

ISSN

0016-6731

Authors

Cole, Joanne B
Manyama, Mange
Larson, Jacinda R
et al.

Publication Date

2017-02-01

DOI

10.1534/genetics.116.193185

Peer reviewed

Human Facial Shape and Size Heritability and Genetic Correlations

Joanne B. Cole,* Mange Manyama,[†] Jacinda R. Larson,^{*,§} Denise K. Liberton,^{*,§} Tracey M. Ferrara,*
Sheri L. Riccardi,* Mao Li,** Washington Mio,** Ophir D. Klein,^{††,**,§§} Stephanie A. Santorico,^{*,***}

Benedikt Hallgrímsson,^{*,§} and Richard A. Spritz^{*,†††,1}

*Human Medical Genetics and Genomics Program, and †††Department of Pediatrics, University of Colorado School of Medicine, Aurora, Colorado 80045, †Department of Anatomy, Catholic University of Health and Allied Sciences, Mwanza, TZ-18, Tanzania, ‡Department of Anatomy and Cell Biology, and §McCaug Institute for Bone and Joint Health, Alberta Children's Hospital Research Institute, Cumming School of Medicine, University of Calgary, T2N 1N4, Canada, **Department of Mathematics, Florida State University, Tallahassee, Florida 32304, ††Department of Orofacial Sciences, †††Department of Pediatrics, and §§Program in Craniofacial Biology, University of California, San Francisco, California 94143, and ***Department of Mathematical and Statistical Science, University of Colorado Denver, Colorado 80202

ABSTRACT The human face is an array of variable physical features that together make each of us unique and distinguishable. Striking familial facial similarities underscore a genetic component, but little is known of the genes that underlie facial shape differences. Numerous studies have estimated facial shape heritability using various methods. Here, we used advanced three-dimensional imaging technology and quantitative human genetics analysis to estimate narrow-sense heritability, heritability explained by common genetic variation, and pairwise genetic correlations of 38 measures of facial shape and size in normal African Bantu children from Tanzania. Specifically, we fit a linear mixed model of genetic relatedness between close and distant relatives to jointly estimate variance components that correspond to heritability explained by genome-wide common genetic variation and variance explained by uncaptured genetic variation, the sum representing total narrow-sense heritability. Our significant estimates for narrow-sense heritability of specific facial traits range from 28 to 67%, with horizontal measures being slightly more heritable than vertical or depth measures. Furthermore, for over half of facial traits, >90% of narrow-sense heritability can be explained by common genetic variation. We also find high absolute genetic correlation between most traits, indicating large overlap in underlying genetic loci. Not surprisingly, traits measured in the same physical orientation (*i.e.*, both horizontal or both vertical) have high positive genetic correlations, whereas traits in opposite orientations have high negative correlations. The complex genetic architecture of facial shape informs our understanding of the intricate relationships among different facial features as well as overall facial development.

KEYWORDS heritability; facial shape; facial size; morphometrics; complex traits

HUMAN appearance is comprised of a remarkably variable set of physical traits. Of all externally visible characteristics, facial appearance is both the most morphologically variable and the most distinctive and recognizable. Facial appearance involves a major genetic component, with each of the many structural features that define facial shape and

appearance themselves likely determined by a multiplicity of genes, with environmental variables such as nutrition and environmental toxins, exerting increasing influence over time (Fitzgerald *et al.* 2010). Nevertheless, the striking similarity of facial appearance within families, often across many generations, suggests that certain key genes exert particularly large effects on facial shape and appearance.

Facial shape is measured in various ways, including specific linear measurements between defined morphological points as well as complex quantitative measurements of the entire face. Previous estimates of the heritability of facial shape distances and angles were principally derived by direct measurements between common facial morphometric landmarks on human faces, cephalograms, and skulls. These estimates

Copyright © 2017 by the Genetics Society of America
doi: 10.1534/genetics.116.193185

Manuscript received June 27, 2016; accepted for publication December 8, 2016;
published Early Online December 14, 2016.

Supplemental material is available online at www.genetics.org/lookup/suppl/doi:10.1534/genetics.116.193185/-/DC1.

¹Corresponding author: University of Colorado School of Medicine, Anschutz Medical Campus, Rm. 3100, Mail-stop 8300, 12800 East 19th Ave., Aurora, CO 80045.
E-mail: richard.spritz@ucdenver.edu

vary widely; in general, facial height dimensions tend to be more heritable than width (Manfredi *et al.* 1997; Carson 2006; Amini and Borzabadi-Farahani 2009; AlKhudhairi and AlKofide 2010), in contrast with the rest of the skull, for which heritability of width tends to be greater than for height (Martínez-Abadías *et al.* 2009a,b, 2012).

The genetic architecture of facial shape variation has been studied more extensively in mice than in humans. In the mouse, measures of craniofacial morphology are highly heritable (Leamy 1977; Klingenberg and Leamy 2001; Klingenberg *et al.* 2001; Percival *et al.* 2016). Further, the mouse skull is highly integrated in terms of phenotypic and genetic correlations (Leamy 1977; Cheverud 1982). Genetic and environmental correlations also tend to be similar, likely due to their basis in similar developmental connections among traits (Cheverud 1982).

Morphological assessment of facial variation has typically required manual landmarking, an approach that is slow, labor intensive, and error prone; complicating its application to large-scale studies as well as comparisons across multiple studies. As an advance toward standardized, replicable phenotyping of human facial traits, we combined advanced three-dimensional (3D) imaging technology with a novel automated landmarking method (Li *et al.* 2016) to derive precise, detailed, and informative facial phenotypes from 29 standard facial morphometric landmarks (Supplemental Material, Table S1) (Bookstein 1997).

Our study, based on Bantu children from Tanzania, avoids facial shape variation that occurs later in life due to injury, weight gain, and disease. Moreover, these African children are very lean, with minimal variation related to facial adiposity, and furthermore have significant occult relatedness, providing the opportunity to formally analyze the heritability of facial shape phenotypes in this population.

To assess heritability, we analyzed genotypes of >15 million common SNPs with minor allele frequencies >1% using Genome-wide Complex Trait Analysis (GCTA) (Yang *et al.* 2010, 2011). We estimated narrow-sense heritability (h^2); heritability explained by common genetic variation (h_g^2); and pairwise genetic correlations of 38 facial phenotypes, incorporating close family structures into a joint linear mixed model with two variance components, one representing the genetic relatedness between close relatives and the other representing the genetic relatedness between all individuals in the study (Zaitlen *et al.* 2013). The phenotypic variance was then partitioned into variance explained by common genetic variation, variance explained by close genetic relationships but not common genetic variation, and the remaining residual variance explained by the environment.

We found that facial shape and size phenotypes are highly heritable, and additionally are highly genetically correlated, and that a large fraction of the genetic component of facial differences can be explained by common variation genome-wide. Our findings help elucidate the complex genetic relationships and pathways underlying facial shape, augment basic biological understanding of facial development, enable better modeling of facial shape based on genetic correlations, and may assist in delineation and diagnosis of facial dysmorphism syndromes.

Materials and Methods

Study subjects

Samples and data were collected from 3631 Bantu African children aged 3–21 over a 3-year period in the Mwanza region of Tanzania. Subjects with a known birth defect or a relative with known orofacial cleft or facial birth defect were excluded. Additional data collected were age, sex, height, weight, head circumference, school, and detailed parental and grandparental ethnicity, and tribe information. Subjects with non-Bantu tribal ancestry in one or more grandparents were excluded from the study. Written informed consent was obtained from all study subjects or their parents as appropriate.

3D facial imaging and automated landmarking

3D images were obtained using the Creaform MegaCapturor 3D photogrammetry imaging system. Each subject was imaged twice at six standard positions. Meshes were reconstructed at the highest possible resolution and assembled using Inspeck software to form a complete 3D mesh of the face (Figure 1).

A set of 29 morphometric facial landmarks (Figure 1 and Table S1) was applied to each individual facial mesh using a novel automated landmarking method (Li *et al.* 2016). Briefly, this method morphs a 29-landmark template (created from a training set of manually landmarked faces) to each individual face through the guidance of anchor points defined by the local curvature features of the face. Presenting the same image to the automated landmarking system twice generates identical landmark positions. Errors, when they occur, tend to be fairly large, readily detectable, and easily removed.

Derivation of phenotypic variables

Landmarks were subjected to Procrustes superimposition for geometric morphometric analysis (Bookstein 1997; Dryden and Mardia 1998; Mitteroecker and Gunz 2009). Superficial artifacts (smiling, squinting, mouth open, lateral nasal deformity, *etc.*) were identified by manual quality inspection of each facial mesh, and were corrected using a multiple linear model in which all factors and their interactions were considered. For each correction, we determined the significance of the artifact using a Procrustes distance permutation test on age- and size-adjusted data. We performed the corrections jointly using a linear model in *R* to avoid overcorrection caused by overlap among the artifacts. Additionally, we determined whether the corrections affected biological signals such as the estimates of ontogenetic or static allometry and the heritabilities of the traits. For all artifacts, we performed canonical variate analysis both before and after to visualize the effect of the correction (Figure S1 and Figure S2).

An additional artifact in 3D photogrammetry is “skew,” defined as coordinated asymmetric displacement of landmarks due either to variation in assembly of the facial views to produce the assembled mesh or from parallax. Most landmarks are affected by skew when it occurs, but individuals are not equally affected. Therefore, we regressed the landmark data on the principal component (PC) scores for PCs

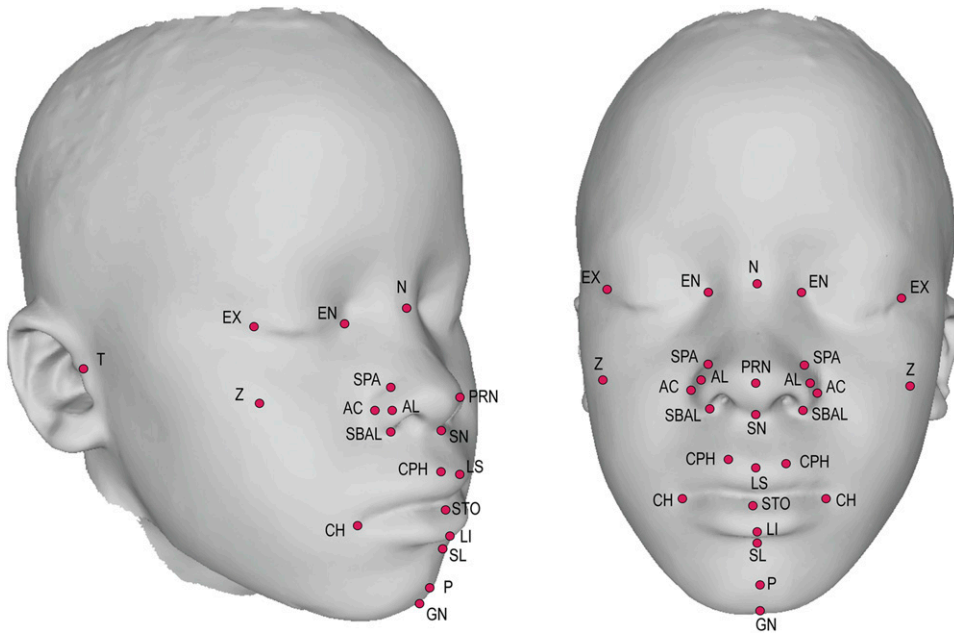


Figure 1 3D facial scan with annotated landmarks. Landmarks annotated are defined in Table S1.

corresponding to skew variation. Skew corrections have minimal effects on most subjects but graded effects on those toward the ends of the skew PC. [Figure S2](#) shows morphs that correspond to the extreme skew values in the sample. Skew corrections were applied to the linear distances as this improved heritability, but not to the multivariate measures as this did not affect heritability. We validated artifact and skew corrections by determining their influences on the estimates of allometric shape variation and on heritabilities.

We obtained 25 linear distance phenotypes representing heights, widths, and depths of different facial structures from the fully corrected landmark coordinates after restoring size. Size was calculated as centroid size, as is standard in geometric morphometrics (Mitteroecker and Gunz 2009). [Table S2](#) lists means and standard deviations for all linear distances and centroid size.

Multivariate measures were calculated from artifact but not skew-corrected data. We removed variation related to age and size in symmetrized landmark data using multiple multivariate regression and centering the residuals on the sample mean (Klingenberg and Zimmermann 1992; Klingenberg 1998). Symmetrizing the data removes facial asymmetry variation. While there is biological variation in asymmetry, this did not significantly affect the first 10 PCs, aside from the skew artifacts discussed above. The age-shape relationship is nonlinear, particularly when an analysis includes both young children and adults. Within our sample, however, polynomial fits for age or centroid size did not significantly improve the fit ([Figure S3](#)). As our sample mostly excludes the major shape changes occurring early in facial growth and the slowing of changes that occur in late ontogeny, linear regression sufficiently captures the shape variation associated with age and centroid size. Shape variation related to size, or static allometry, was estimated using the regression

scores corresponding to size independent of age. We obtained the scores for the first 10 PCs based on the age and size-standardized landmark coordinate data ([Figure S4](#)). All references to PCs in the results refer to the PC scores derived from the phenotypic data.

We used Klingenberg's permutation test for Escoffier's RV coefficient to identify the set of spatially contiguous landmarks that maximized the ratio of covariation among themselves to covariation with landmarks outside of that set (Klingenberg 2009). This method does not consider overlapping determinants of covariation structure (Hallgrímsson *et al.* 2009), but it reveals sets of strongly covarying, spatially adjacent landmarks. The resulting set, defined by the nasal region and upper lip ([Figure S5](#)), was subjected to separate Procrustes alignment, and a principal component analysis (PCA). The first PC (40% of variance) served as a measure of variation within this "module."

The final phenotype values then adjusted for biological covariates as follows: multivariate measures including all PCs and allometry were adjusted for sex; linear distances were adjusted for age, sex, and centroid size (after age-sex adjustment); and centroid size was adjusted for age and sex. In this way, all multivariate measures and linear distances were corrected for age, sex, and size prior to downstream analysis. Phenotypic correlations used throughout are based on phenotype residual correlations on a subset of unrelated individuals. All morphometric analyses were done in MorphoJ (Klingenberg 2011) or in *R* using the Geomorph (Adams and Otárola-Castillo 2013; Adams *et al.* 2014) and Morpho (Schlager 2016) packages.

Genome-wide genotyping and quality control

Genome-wide genotyping, quality control, and imputation of 3480 study subjects used in these analyses were described previously (Cole *et al.* 2016). The final postquality-control

dataset included 3480 individuals with complete phenotyping information and imputed genotypes at >15 million markers with INFO scores >0.30. A sensitivity analysis comparing heritability estimates from the full imputed data set and from a data set of only genotyped markers demonstrated no bias in using imputed genotypes (Figure S6).

Heritability estimates

Both h^2 and h_g^2 were estimated using GCTA software (Yang *et al.* 2010, 2011). We fit a joint linear mixed model with two variance components for each phenotype as described (Zaitlen *et al.* 2013). Briefly, one variance component represented close relatives only, in which any pairwise genetic correlation in the full genetic relatedness matrix as calculated by GCTA <0.05 was set to 0. Specifically, our variance component highlighting close relationships contained 4425 pairwise relationships ≥ 0.05 from a total of 2937 individuals in each triangle half of the matrix. While this variance component represents a small proportion of all pairwise relationships in our sample (0.07%), it includes 84% of our total sample. Therefore the “missing heritability” explained by this additional variance component of close relatives is based on a large number of independent nuclear families, and thus is not biased by a small number of large families (Figure S7). Heritability estimates obtained using different relatedness thresholds demonstrated that 0.05 was both unbiased and conservative when compared to 0.00 and 0.025. The other variance component represented the full genetic relatedness matrix for all individuals. The joint model uses 4,307,014 more pairwise comparisons from 3480 individuals to estimate h_g^2 than the traditional GCTA unrelateds only model ($n = 1869$), using their recommended relatedness threshold cutoff value of 0.025 (Table S3) (Yang *et al.* 2010). GCTA uses restricted maximum likelihood to estimate the variance of each component, the sum of which represents total genetic variance, used for calculating h^2 . By default, GCTA estimates that escape from the parameter space were set to $1.0 \times 10^{-6} \times$ phenotypic variance. To adjust our significance threshold for multiple testing of correlated phenotypes, we performed PCA of the 38 phenotype residuals in unrelated individuals to determine the number of effectively independent phenotypes. The first 11 eigenvectors had eigenvalues >1, making them each representative of at least one phenotype. We divided the traditional $P < 0.05$ threshold by 11, making our significance threshold $P < 0.0045$.

To calculate heritabilities and genetic variances for each landmark, we obtained the genetic and phenotypic variance-covariance matrices for the symmetrized landmarks. This leaves out one dimension for midline landmarks and treats the landmark coordinates for both sides as a single variable. Heritabilities are calculated as the ratio of genetic to phenotypic variance for each landmark coordinate. We then used a heatmap method to visualize these variance components across the face. Here, each component is represented as a vector that has a length proportional to the variance component, an origin at each landmark, and a direction parallel to a vector that connects each landmark to the landmark centroid. These vectors are then used to produce a face morph using the

thin-plate-spline method that is then superimposed on the unmorphed mean face to generate a heatmap.

Genetic correlation

Genetic correlations between all phenotypes were also estimated using GCTA software (Yang *et al.* 2011). We eliminated PC8 and LS_STO, for which the joint heritability LRT models were not significant (Table 2), from the genetic correlation matrix. Due to nonconvergence of such a large parameter space, 148/630 bivariate analyses failed the joint analysis and instead, for the sake of having a complete genetic correlation matrix, were fit by the standard GCTA approach, using a single genetic relatedness matrix of only unrelated individuals ($n = 1869$). Of those 148 bivariate models, 36 failed the single component model of unrelateds due to constraining genetic or environmental components. To construct a complete genetic correlation matrix, we estimated these 36 values based on both univariate and bivariate models of the traits affected. If the bivariate model's genetic component was constrained or the univariate model's heritability estimate was less than the SE of that estimate, we set the genetic covariance to $1.0 \times 10^{-6} \times$ phenotypic covariance. If the bivariate model's environmental component was constrained or the univariate model's heritability was essentially equal to one, we set the genetic covariance as equal to the total phenotypic covariance between the two traits. Therefore, the genetic correlation matrix represents only the shared genetic correlation which can be explained by >15 million common variants. Table S4 includes all h_g^2 genetic correlation estimates, SE, and models in which those values were derived.

Data availability

Phenotype data were deposited in FaceBase (<https://www.facebase.org/>; accession number: FB00000667.01). Genotype data were deposited in the Database of Genotypes and Phenotypes (dbGaP) (<http://www.ncbi.nlm.nih.gov/gap>; accession number: phs000622.v1.p1). This study was carried out with overall approval and oversight of the Colorado Multiple Institutional Review Board (protocol #09-0731), was additionally approved by the institutional review boards of the University of Calgary, Florida State University, the University of California San Francisco, and the Catholic University of Health and Allied Sciences (Mwanza, Tanzania), and was carried out with the approval of the National Institute for Medical Research (Tanzania).

Results

Study population and phenotypes

The study population consisted of 3480 normal African Bantu children and adolescents ages 3–21 from the Mwanza region of Tanzania. Over 70% of subjects were aged 7–12, and 44.4% were male and 55.6% female (Figure 2). As described previously (Cole *et al.* 2016), PCA of population substructure demonstrated minimal genetic clustering and an analysis of fixation index demonstrated no apparent subgroups by school or tribe.

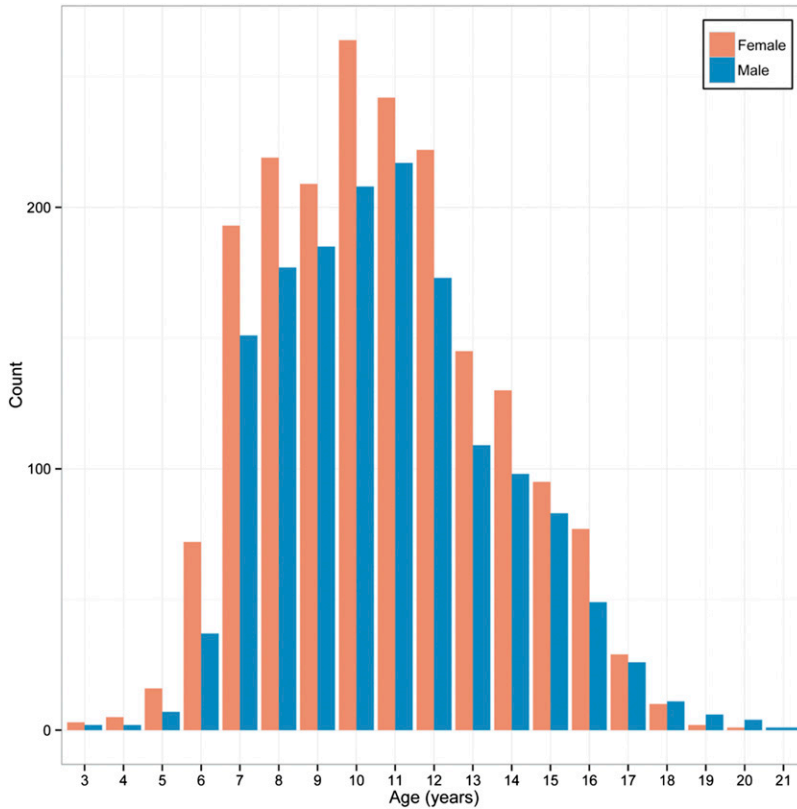


Figure 2 Study age distribution by sex.

For each subject, we captured 3D facial scans, applied 29 standard facial morphometric landmarks (Figure 1 and Table S1) (Bookstein 1997), derived 38 facial shape phenotypes based on the landmarks, carried out genome-wide SNP genotyping, and used these data to estimate h^2 and h^2_g for each phenotype. These facial phenotypes represent several different classes, including 3D summary variables in the form of PCs derived from PCA of the whole face and PCA of the most highly correlated landmarks positioned around the midface, interlandmark linear distances, and global measures of overall facial size and the relationship between size and shape (Table 1). In addition, for each subject we obtained height and weight, from which we calculated body mass index (BMI). Analysis of these data showed that the mean BMI of the study population was ~ 1 SD below the 2007 World Health Organization world standards (Figure S8). Furthermore, the correlations between all age- and sex-adjusted facial traits with age- and sex-adjusted BMI in unrelated individuals are small ($r^2 = -0.18$ to 0.14), suggesting that BMI is not a confounding factor in our study population.

Heritability of facial phenotypes

As shown in Figure 3 and Table 2, 36 of our 38 phenotypes were significantly heritable ($P < 0.0045$), with h^2 28.3–66.9%. The most heritable facial traits include PC7, representing nasal root shape and mouth width ($h^2 = 66.9\%$, $SE = 7.2\%$); total facial width (T_R_T_L) ($h^2 = 66.2\%$, $SE = 7.5\%$); the allometric variable ($h^2 = 64.3\%$, $SE = 7.2\%$); centroid size ($h^2 = 64.1\%$,

$SE = 7.6\%$); and nasion to midendocanthion distance (N_MEN) ($h^2 = 63.9\%$, $SE = 7.5\%$). Furthermore, by combining genetic variance across all 10 orthogonal PCs, which explain $>87\%$ of total shape variation captured by sparse landmarking (Figure S4), we obtained a single global estimate of total facial shape of $h^2 = 50.1\%$. Previous studies have suggested that vertical measures have greater heritability than horizontal measures (Manfredi *et al.* 1997; Carson 2006; Amini and Borzabadi-Farahani 2009; AlKhudhairi and AlKofide 2010). However, we observed a trend toward horizontal facial measures having greater heritability than vertical measures. Figure 4 depicts h^2 and h^2_g estimates for the 25 linear distances, clustered by physical orientation and phenotypic correlation. The three facial depth measurements, lower facial depth (GN_T), midfacial depth (SN_T), and upper facial depth (N_T), share the tragion landmark and have very similar h^2 estimates ($h^2 = 48.6\%$, $SE = 7.6\%$; $h^2 = 48.7\%$, $SE = 7.6\%$; and $h^2 = 51.2\%$, $SE = 7.6\%$; respectively), but exhibit very different phenotypic correlations (GN_T:SN_T = 0.31, GN_T:N_T = -0.04 , and SN_T:N_T = 0.67). Similarly, the three horizontal eye measurements, inner canthal distance (EN_R_EN_L), outer canthal distance (EX_R_EX_L), and average palpebral fissure length (EN_EX), likewise share some landmarks in common and have fairly similar h^2 estimates, ($h^2 = 41.1\%$, $SE = 7.6\%$; $h^2 = 52.2\%$, $SE = 7.6\%$; and $h^2 = 56.6\%$, $SE = 7.8\%$; respectively), but exhibit very different phenotypic correlations (EN_R_EN_L:EX_R_EX_L = 0.49, EN_R_EN_L:EN_EX = -0.03 , and EX_R_EX_L:EN_EX = 0.82). In contrast, three midfacial horizontal measures, mouth

Table 1 The 38 facial phenotypes derived from landmarks on 3D facial scans

| Phenotype abbreviation | Physical description |
|--|--|
| PCA | |
| PC1 | upper facial height, midfacial width |
| PC2 | overall facial height, lower facial height |
| PC3 | upper and middle facial width |
| PC4 | width of the nose, mandible height |
| PC5 | nose shape, height of the mouth |
| PC6 | nasal width, maxillary prognathism |
| PC7 | nasal root shape, mouth width |
| PC8 | cheek protrusion |
| PC9 | midface protrusion, upper facial height |
| P10 | chin height, nasion protrusion |
| PC1 from a PCA of the midfacial landmark network (MidfaceModPC1) | midfacial landmark network around the nose and mouth |
| Size-related measurements | |
| Centroid size | facial size |
| Allometry | variation in shape due to size |
| Linear distances ^a | |
| AL_R_AL_L | nasal width |
| AC_PRN | nasal ala length (average) |
| CH_R_CH_L | mouth width |
| CPH_R_CPH_L | philtrum width |
| EN_EX | palpebral fissure length (average) |
| EN_R_EN_L | inner canthal width |
| EX_R_EX_L | outer canthal width |
| GN_T | lower facial depth (average) |
| LI_SL | cutaneous lower lip height |
| LS_STO | upper vermilion height |
| N_GN | morphological facial height |
| N_MEN | nasion to midendocanthion |
| N_PRN | nasal bridge length |
| N_SN | nasal height |
| N_STO | upper facial height |
| N_T | upper facial depth (average) |
| SBAL_R_SBAL_L | subnasal width |
| SN_GN | lower facial height |
| SN_LS | philtrum length |
| SN_PRN | nasal protrusion |
| SN_STO | upper lip height |
| SN_T | midfacial depth (average) |
| STO_LI | lower vermilion height |
| STO_SL | lower lip height |
| T_R_T_L | facial width |

^a Linear distances are the distance between two landmarks (e.g., AL_R and AL_L).

width (CH_R_CH_L), philtrum width (CPH_R_CPH_L), and subnasal width (SBAL_R_SBAL_L), share no overlapping landmarks, have similar h^2 estimates ($h^2 = 37.8\%$, SE = 7.7%; $h^2 = 33.7\%$, SE = 7.7%; and $h^2 = 37.2\%$, SE = 8.0%; respectively), and also exhibit fairly high phenotypic correlations (CH_R_CH_L:CPH_R_CPH_L = 0.55, CH_R_CH_L:SBAL_R_SBAL_L = 0.62, and CPH_R_CPH_L:SBAL_R_SBAL_L = 0.48). It appears that facial traits of similar orientation that either share overlapping morphological points or have high phenotypic correlations are influenced by additive genetic effects and environmental effects to similar degrees.

Figure 5 shows the anatomic distribution of phenotypic and genetic variance as well as heritability by landmark. The pattern is consistent with Figure 3 and Figure 4 in that the

landmarks defining facial width and the orbital region tend to have higher genetic variances and heritabilities.

Genetic basis of observed heritability

For 22 of the 38 facial phenotypes analyzed, >90% of the narrow-sense heritability (h^2) can be explained by the effects of common genetic variation (h_g^2/h^2). However, for a number of other traits, common variation (h_g^2) accounts for <50% of h^2 ; indicating significant additional genetic contributions beyond common variants that can be imputed for Africans from the Illumina HumanOmni 2.5-8 array, which captures 54% of common African variation (minor allele frequency >1%; <http://www.illumina.com/content/dam/illumina-marketing/documents/products/datasheets/datasheet-human-omni2.5-exome-8.pdf>). However, we caution that these conclusions

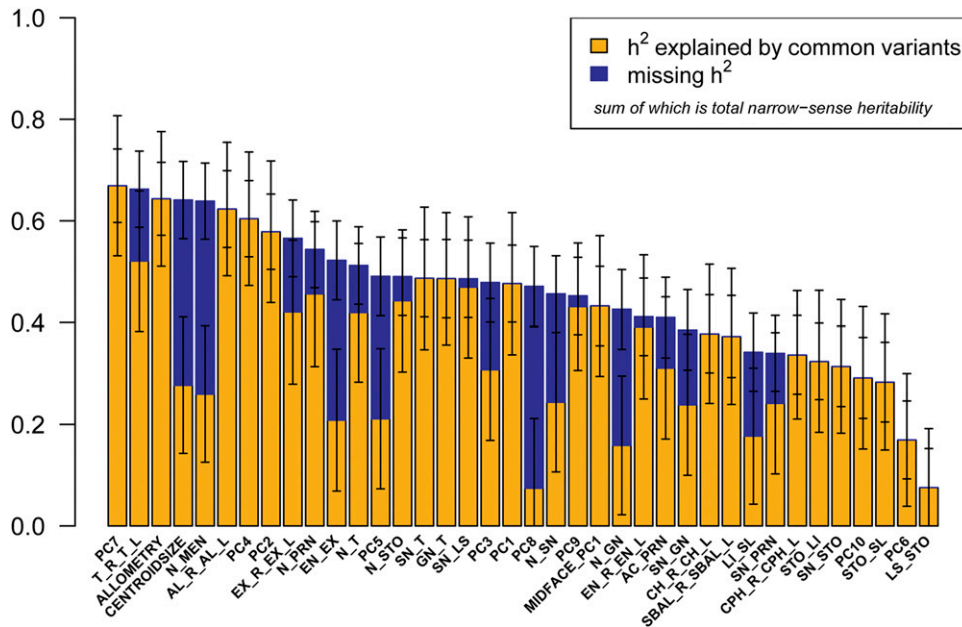


Figure 3 Heritability of 38 facial traits. The bar plot represents h^2_g (yellow), missing h^2 (blue), and total h^2 (yellow + blue) with error bars for all 38 facial phenotypes analyzed. Bars that apparently have no missing h^2 (blue) indicate that h^2_g equals h^2 ; therefore, narrow-sense heritability of that phenotype can be explained fully by common genetic variation.

are based on estimates of h^2_g/h^2 that have high SE (Table 2). These traits include centroid size, nasion to midendocanthion (N_MEN), palpebral fissure length (EN_EX), PC5 representing nose shape and height of the mouth, PC8 representing cheek protrusion, and morphological facial height (N_GN).

To elucidate underlying genetic relationships between different facial traits, we estimated pairwise genetic correlations between all significantly heritable traits (Table S4) and constructed a genetic correlation matrix of all significantly heritable linear distances (Figure 6). Due to lack of power to detect h^2 in joint bivariate models between all traits (Visscher *et al.* 2014), these genetic correlations are based on the genetic covariance calculated from >15 million common variants and not total genetic covariance, resulting in higher SE. Although not all genetic correlation estimates are significantly different from 0 ($P < 0.05$), Figure 6 depicts striking patterns of shared heritability among distinct facial traits. A number of horizontal measurements mostly defined by nonoverlapping landmarks have high positive genetic correlations with each other. These phenotypes include palpebral fissure length (EN_EX), outer canthal width (EX_R_EX_L), facial width (T_R_T_L), mouth width (CH_R_CH_L), subnasal width (SBAL_R_SBAL_L), philtrum width (CPH_R_CPH_L), and two PCs that both account for midfacial width (PC1 and MidfaceModPC1). We observed a similar pattern of high positive genetic correlations, though to a lesser extent, among midline vertical measurements. These include upper lip height (SN_STO), morphological facial height (N_GN), upper facial height (N_STO), PC2 representing both overall and lower facial height, lower lip height (STO_SL), and philtrum length (SN_LS). Importantly, the horizontal and vertical measurements exhibit large negative genetic correlations with each other, indicating that phenotypic variation along both horizontal and vertical measurements are largely

caused by the same genetic variation acting to increase one direction while decreasing the other. In a simple sense, this means that the same alleles that cause an individual to have a broad face also cause that individual to have a short face, and vice versa.

Discussion

We report here the first estimates of both heritability and genetic correlation of facial shape phenotypes derived from 3D facial scans and true genome-wide genetic correlations between 1000s of individuals. Facial scans provide far more accurate measurements than previous approaches based on direct manual measurements between prominent facial features (Ozsoy *et al.* 2009). Furthermore, direct calculation of genome sharing from genome-wide data are more accurate than kinship coefficients used in traditional heritability analyses, which represent the average genetic sharing for any given relationship and not the actual genetic correlation for any specific pair of relatives (Hayes *et al.* 2009).

Our analysis, carried out in Bantu children from Tanzania, provides the opportunity to assess heritability of facial shape and size in a young, lean population. The choice of population is both a strength and a limitation of this analysis. In any population, heritability is determined by a combination of genetic variance and environmental influences. Variation in facial adiposity, for instance, is small in this population while it may be large in others (Figure S8) (Cole *et al.* 2016). The focus on children creates the need to adjust for age and size but also avoids facial shape changes that occur later in life due to injury, weight gain, and disease.

Not surprisingly, we found that many quantitative facial-shape phenotypes, derived with high accuracy from 3D facial

Table 2 Heritability of 38 facial traits

| Trait | h_g^2 | SE (h_g^2) | h^2 | SE (h^2) | LRT P -value ^a | h_g^2/h^2 | SE (h_g^2/h^2) |
|---------------|---------|----------------|-------|--------------|-----------------------------|-------------|--------------------|
| PC7 | 0.669 | 0.138 | 0.669 | 0.072 | 1.00×10^{-17b} | 1.000 | 0.560 |
| T_R_T_L | 0.521 | 0.138 | 0.662 | 0.075 | 1.00×10^{-17b} | 0.786 | 0.482 |
| Allometry | 0.643 | 0.132 | 0.643 | 0.072 | 1.00×10^{-17b} | 1.000 | 0.562 |
| Centroid Size | 0.277 | 0.134 | 0.641 | 0.076 | 3.66×10^{-15} | 0.432 | 0.335 |
| N_MEN | 0.260 | 0.134 | 0.639 | 0.075 | 3.89×10^{-16} | 0.406 | 0.322 |
| AL_R_AL_L | 0.623 | 0.131 | 0.623 | 0.076 | 1.00×10^{-17b} | 1.000 | 0.575 |
| PC4 | 0.604 | 0.131 | 0.604 | 0.075 | 5.55×10^{-17} | 1.000 | 0.583 |
| PC2 | 0.579 | 0.139 | 0.579 | 0.074 | 1.00×10^{-17b} | 1.000 | 0.607 |
| EX_R_EX_L | 0.421 | 0.141 | 0.566 | 0.076 | 8.11×10^{-14} | 0.744 | 0.509 |
| N_PRN | 0.456 | 0.142 | 0.544 | 0.075 | 3.94×10^{-15} | 0.839 | 0.562 |
| EN_EX | 0.208 | 0.140 | 0.522 | 0.078 | 4.35×10^{-10} | 0.399 | 0.360 |
| N_T | 0.419 | 0.136 | 0.512 | 0.076 | 4.52×10^{-14} | 0.819 | 0.564 |
| PC5 | 0.211 | 0.138 | 0.491 | 0.077 | 6.33×10^{-10} | 0.430 | 0.385 |
| N_STO | 0.443 | 0.140 | 0.490 | 0.076 | 2.22×10^{-13} | 0.903 | 0.621 |
| GN_T | 0.487 | 0.140 | 0.487 | 0.076 | 2.97×10^{-12} | 1.000 | 0.663 |
| SN_LS | 0.486 | 0.130 | 0.486 | 0.077 | 5.26×10^{-11} | 1.000 | 0.651 |
| SN_T | 0.469 | 0.139 | 0.486 | 0.076 | 2.97×10^{-13} | 0.966 | 0.650 |
| PC3 | 0.308 | 0.139 | 0.478 | 0.078 | 2.03×10^{-10} | 0.643 | 0.504 |
| PC1 | 0.477 | 0.140 | 0.477 | 0.076 | 5.76×10^{-13} | 1.000 | 0.672 |
| PC8 | 0.074 | 0.137 | 0.471 | 0.079 | 2.50×10^{-8} | 0.158 | 0.223 |
| N_SN | 0.244 | 0.137 | 0.456 | 0.075 | 1.95×10^{-10} | 0.535 | 0.455 |
| PC9 | 0.431 | 0.125 | 0.452 | 0.076 | 1.16×10^{-13} | 0.953 | 0.643 |
| MidfaceModPC1 | 0.433 | 0.138 | 0.433 | 0.078 | 2.23×10^{-9} | 1.000 | 0.706 |
| N_GN | 0.159 | 0.137 | 0.426 | 0.078 | 1.11×10^{-7} | 0.373 | 0.380 |
| EN_R_EN_L | 0.392 | 0.142 | 0.411 | 0.076 | 2.09×10^{-9} | 0.952 | 0.699 |
| AC_PRN | 0.311 | 0.140 | 0.410 | 0.079 | 1.47×10^{-7} | 0.758 | 0.604 |
| SN_GN | 0.239 | 0.139 | 0.386 | 0.079 | 8.70×10^{-7} | 0.619 | 0.546 |
| CH_R_CH_L | 0.378 | 0.137 | 0.378 | 0.077 | 7.99×10^{-6} | 1.000 | 0.747 |
| SBAL_R_SBAL_L | 0.373 | 0.134 | 0.373 | 0.080 | 2.76×10^{-6} | 1.000 | 0.754 |
| LI_SL | 0.177 | 0.134 | 0.342 | 0.077 | 5.61×10^{-6} | 0.518 | 0.510 |
| SN_PRN | 0.242 | 0.139 | 0.340 | 0.074 | 1.37×10^{-6} | 0.711 | 0.629 |
| CPH_R_CPH_L | 0.337 | 0.126 | 0.337 | 0.077 | 3.45×10^{-6} | 1.000 | 0.775 |
| STO_LI | 0.324 | 0.139 | 0.324 | 0.075 | 2.48×10^{-5} | 1.000 | 0.810 |
| SN_STO | 0.314 | 0.131 | 0.314 | 0.079 | 1.57×10^{-5} | 1.000 | 0.819 |
| PC10 | 0.291 | 0.140 | 0.291 | 0.080 | 0.000570 | 1.000 | 0.860 |
| STO_SL | 0.283 | 0.134 | 0.283 | 0.078 | 0.000102 | 1.000 | 0.863 |
| PC6 | 0.169 | 0.131 | 0.169 | 0.077 | 0.0152 | 1.000 | 1.10 |
| LS_STO | 0.076 | 0.116 | 0.076 | 0.077 | 0.259 | 1.000 | 1.61 |

h^2 , h_g^2 , and the proportion of narrow-sense heritability explained by common genetic variants (h_g^2/h^2), all with SE.

^a LRT P -value for the joint model vs. the null model ($H_0: h^2 = 0$).

^b LRT P -value was reported as 0, indicating it was less than the GCTA limit 1×10^{-17} .

scans, are highly heritable. Furthermore, most of these quantitative facial phenotypes can be explained by common genetic variants across the genome. In particular, based on h^2 , several horizontal measurements including facial width (T_R_T_L; $h^2 = 66.2\%$, SE = 7.5%), nasal width (AL_R_AL_L; $h^2 = 62.3\%$, SE = 7.6%), outer canthal width (EX_R_EX_L; $h^2 = 56.6\%$, SE = 7.6%), and palpebral fissure length (EN_EX; $h^2 = 52.2\%$, SE = 7.8%) appear to be among the most heritable facial features; contrary to findings of previous heritability studies of the face. There are several obvious potential explanations for this difference. First, heritability of some facial attributes may be population specific, driven by different underlying genetic variants in different populations; thus reflecting differing underlying biological bases of facial shape and size. Second, the present study population, Tanzanian Bantu children, is a much leaner population than has been studied previously. BMI in our cohort

of Tanzanian Bantu children is significantly lower than world standards (Figure S8) (de Onis *et al.* 2004) and is uncorrelated with our measures of facial shape after adjusting for age, sex, and centroid size (see *Materials and Methods*). Linear measures, particularly horizontal distances, collected in populations with higher BMI, may be more affected by excess subcutaneous fat, reflecting a greater environmental component, and thus proportionately smaller genetic component. Third, genetic influences on horizontal facial distances may be proportionately greater at younger ages, as in our cohort of children and adolescents ages 3–21, whereas these distances may become proportionately more affected by environmental components with increasing age. This model of age-related shape differences fits well with what is already known about how the face matures and morphs into the adult form. As the face reaches adult shape at ~ 16 years of age (as determined in males of

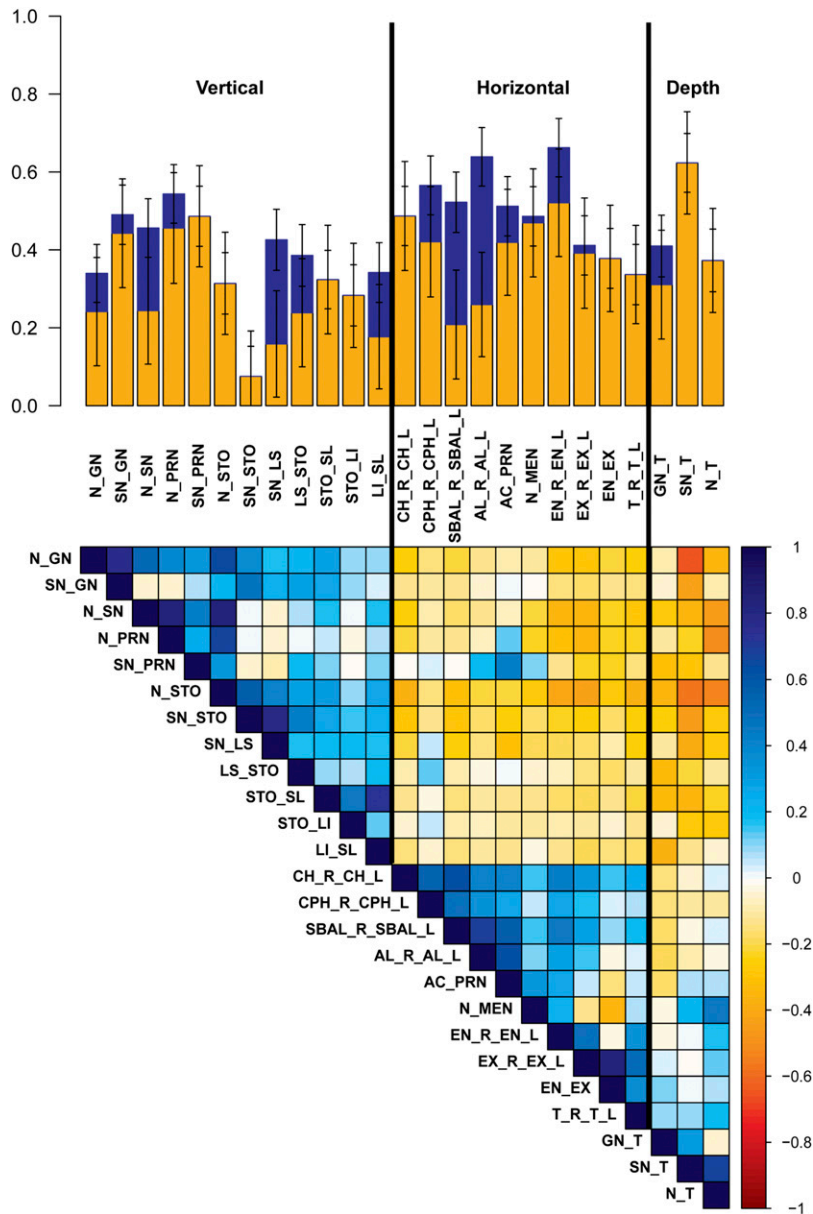


Figure 4 Heritability of linear distances by measurement orientation. The bar plot represents h_g^2 (yellow), missing h^2 (blue), and total h^2 (yellow + blue) with error bars for 25 linear distances. Traits are first clustered by orientation, then by facial structure with between-trait phenotypic correlations seen in the colored matrix in the bottom half of the figure.

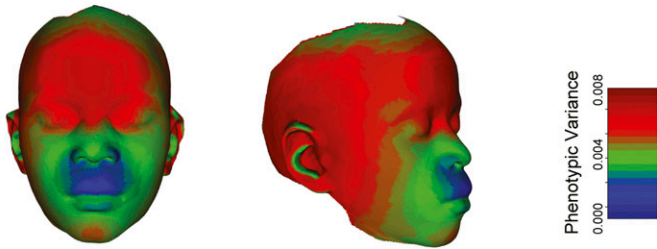
European descent), the midface undergoes a strong vertical expansion and becomes relatively taller than the rest of the face (Bastir *et al.* 2006).

The 10 PCs displayed similar heritabilities as the linear distances. PCs represent axes of covariation within the data and most combine variation from multiple if not most landmarks. A limitation of PCA is that the assumption that each PC is orthogonal to the previous may not map well onto the underlying biological determinants of covariation structure. In the absence of knowledge about those determinants, however, PCA is a widely accepted and rational approach to multivariate data. In this context, each PC represents a distinct facial shape transformation that emerges from the covariance structure of the data and can be treated as a univariate trait.

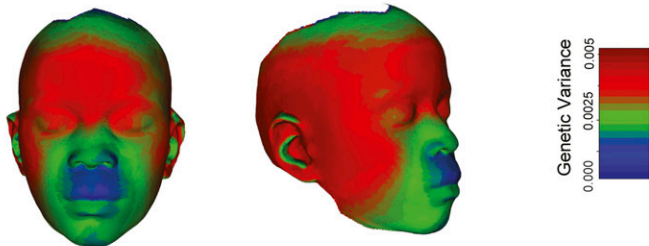
Interestingly, global facial size appears to be among the most heritable of facial traits. Allometry, a measure of the

variation in shape due to size, has h^2 of 64.3% (SE = 7.2%). Centroid size, a measure of overall face size, has h^2 of 64.1% (SE = 7.6%). These findings indicate that there may be a strong genetic basis underlying global size of the face and how size drives shape variation; whereas facial shape *per se*, irrespective of size, may be somewhat more influenced by environmental factors. Although our findings also indicate that the majority of facial shape variation can be explained by the effects of common genetic variation, there were several facial phenotypes, including centroid size, for which h_g^2 did not explain the majority of h^2 . Potential explanations for such missing heritability include variants not in linkage disequilibrium with variants on our array, rare causal genetic variants, uncharacterized structural variation, and epistatic effects. Our genome-wide association studies (GWAS) of

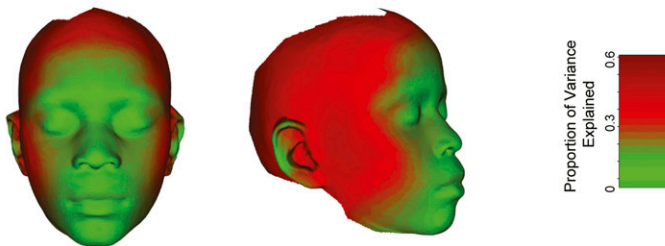
A Anatomical Distribution of Phenotypic Variance



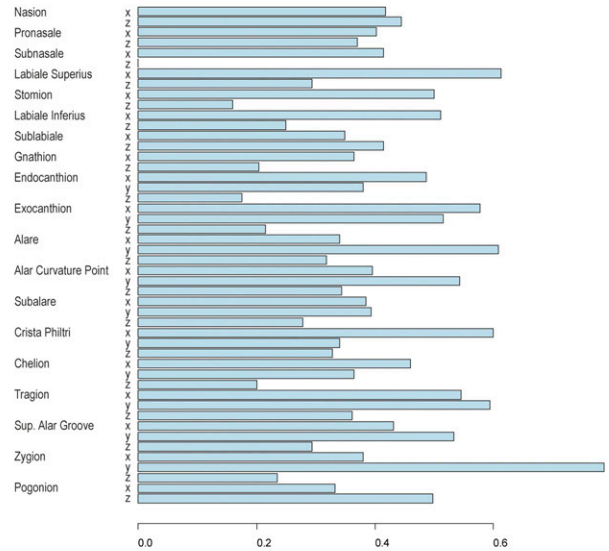
B Anatomical Distribution of Genetic Variance



C Anatomical Distribution of Heritability



D Heritabilities by Landmark and Coordinate



E Vectors Depicting Heritabilities by Landmark as Vectors

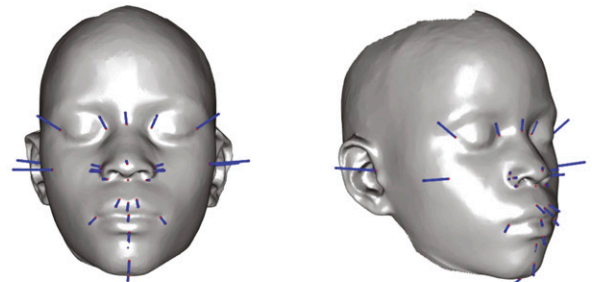


Figure 5 Distribution of variance components across the face. (A–C) The anatomical distribution of phenotypic and genetic variances as well as heritabilities is shown. These are represented as heatmaps based on a thin-plate-spline morph as described in *Materials and Methods*. (D) The heritability estimates or the Procrustes-superimposed symmetrized landmarks are shown. (E) The vectors, magnified 10-fold, used to generate the heritability heatmap are depicted.

these same facial traits in Africans identified two loci that were significantly associated with either centroid size or allometry (Cole *et al.* 2016); traits with high h^2 but variable h_g^2 . While these heritability estimates support an overall genetic contribution, the specific estimate of h_g^2 does not provide information on the magnitude of effect of contributing loci, and thus is not necessarily an indicator of GWAS success. Irrespective of the specific h_g^2 estimates for centroid size and allometry, our GWAS of 6300 individuals had the power to detect genetic determinants with relatively large effect sizes for both traits.

We observed high positive genetic correlations among variables that represent similar orientations on the face, and rather high negative genetic correlations among variables that represent different orientations. The highest genetic correlations, of horizontal measures across the facial midline, likely correspond to related genetic effects on biological relationships underlying facial structure

during development, in which the two sides of the face meet and fuse at the midline (Sperber *et al.* 2001). The negative genetic correlations we observe between horizontal and vertical facial measures are consistent with overall phenotypic correlations between these measures. Furthermore, high positive and negative genetic correlations between a wide array of facial traits support the presence of a finite set of underlying genes involved in overall facial development.

Finally, our analysis of genetic variance and covariance structure shows that genetic variation in the face is both highly integrated and modular. Integration refers to the developmentally based tendencies for traits to covary (Hallgrímsson *et al.* 2009; Klingenberg 2013), while modularity refers to suites of traits connected by development (Wagner *et al.* 2007). We find a large number of both positive and negative correlations among traits, attesting to highly structured patterns of variation. For craniofacial morphology more generally, somatic growth,

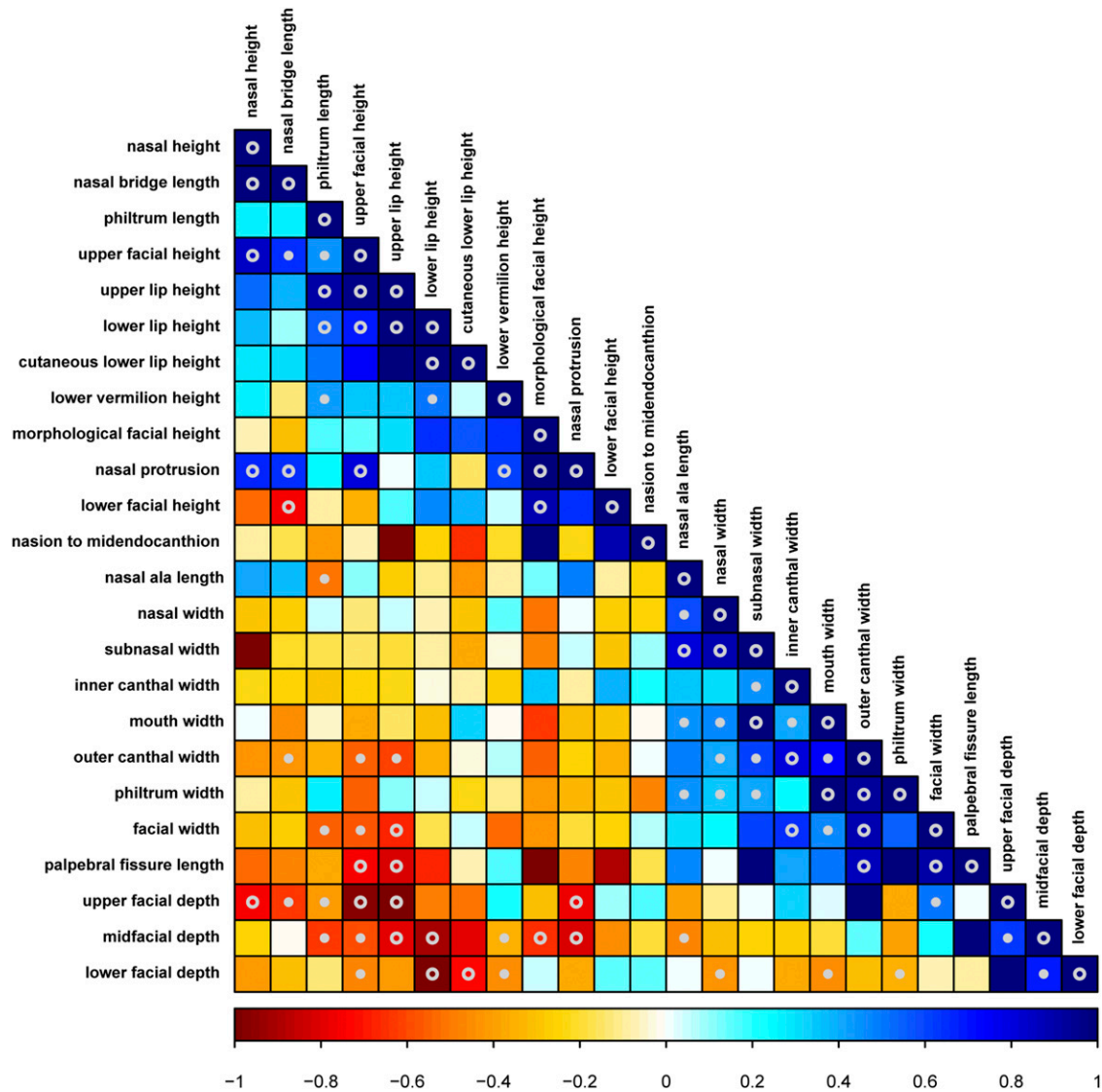


Figure 6 Pairwise genetic correlation matrix of the linear distances. Genetic correlation was calculated from >15 million common genetic variants. Traits that have high positive genetic correlations with each other are shown in blue, indicating that the same genetic loci alter the magnitude of those traits in the same direction. Traits that have high negative genetic correlations with each other are shown in red, indicating that the same genetic loci are contributing to each phenotype in opposite directions, increasing one while decreasing the other. Genetic correlation estimates that are significantly different ($P < 0.05$) from 0 to +1 or 0 to -1 are marked with \circ and genetic correlation estimates that are significantly different ($P < 0.05$) than 0, +1, and -1 are marked with \circ .

chondrocranial growth, and brain growth are known to drive such patterns of integrated variation in both mouse and human crania (Cooper *et al.* 2004; Hallgrímsson *et al.* 2006, 2009; Marcucio *et al.* 2011; Martínez-Abadías *et al.* 2012). Here, both facial size and facial shape allometry exhibit a pattern of genetic correlations with facial measures that capture aspects of facial height, midfacial width, and lower facial prognathism. This pattern of genetic correlations likely reflects the overall influence of somatic growth on facial shape, forming a developmentally based module within the face. Further work integrating developmental studies with results such as these will shed light on the mechanistic basis for the structure of variation in the face.

Acknowledgments

This work was funded by grants from the National Institutes of Health under the National Institute of Dental and Craniofacial Research (NIDCR) FaceBase Initiative (<http://www.nidcr.nih.gov/>; NIDCR DE-020054 to R.A.S.), the Center for Inherited Disease Research (<http://www.cidr.jhmi.edu/>; HG006829 to R.A.S.), the National Institute of Justice (<http://www.nij.gov/Pages/welcome.aspx>; 2013-DN-BX-K005 to R.A.S.), and the National Science and Engineering Council Discovery Grant (http://www.nserc-crsng.gc.ca/index_eng.asp; DG#238992-12 to B.H.). The funders had no role in study design, data collection and analysis, decision to publish, or preparation of the manuscript.

Literature Cited

- Adams, D. C., and E. Otárola-Castillo, 2013 Geomorph: an R package for the collection and analysis of geometric morphometric shape data. *Methods Ecol. Evol.* 4: 393–399.
- Adams, D. C., M. L. Collyer, E. Otárola-Castillo, and E. Sherratt, 2014 Geomorph: Software for geometric morphometric analyses. R package version 2.1. <https://cran.r-project.org/web/packages/geomorph/geomorph.pdf>
- AlKhudhairi, T. D., and E. A. AlKofide, 2010 Cephalometric craniofacial features in Saudi parents and their offspring. *Angle Orthod.* 80: 1010–1017.
- Amini, F., and A. Borzabadi-Farahani, 2009 Heritability of dental and skeletal cephalometric variables in monozygous and dizygous Iranian twins. *Orthod. Waves* 68: 72–79.
- Bastir, M., A. Rosas, and P. O'Higgins, 2006 Craniofacial levels and the morphological maturation of the human skull. *J. Anat.* 209: 637–654.
- Bookstein, F. L., 1997 *Morphometric Tools for Landmark Data: Geometry and Biology*. Cambridge University Press, Cambridge, United Kingdom.
- Carson, E. A., 2006 Maximum likelihood estimation of human craniometric heritabilities. *Am. J. Phys. Anthropol.* 131: 169–180.
- Cheverud, J. M., 1982 Phenotypic, genetic, and environmental integration in the cranium. *Evolution* 36: 499–516.
- Cole, J. B., M. F. Manyama, E. Kimwaga, J. Mathayo, J. R. Larson *et al.*, 2016 Genomewide association study of African children identifies association of *SCHIP1* and *PDE8A* with facial size and shape. *PLoS Genet.* 12: e1006174.
- Cooper, D., J. Matyas, M. Katzenberg, and B. Hallgrímsson, 2004 Comparison of microcomputed tomographic and micro-radiographic measurements of cortical bone porosity. *Calcif. Tissue Int.* 74: 437–447.
- de Onis, M., T. M. A. Wijnhoven, and A. W. Onyango, 2004 Worldwide practices in child growth monitoring. *J. Pediatr.* 144: 461–465.
- Dryden, I. L., and K. V. Mardia, 1998 *Statistical Shape Analysis*. John Wiley & Sons, Chichester, United Kingdom.
- Fitzgerald, R., M. H. Graivier, M. Kane, Z. P. Lorenc, D. Vleggaar *et al.*, 2010 Update on facial aging. *Aesthet. Surg. J.* 30: 11S–24S.
- Hallgrímsson, B., J. J. Brown, A. F. Ford-Hutchinson, H. D. Sheets, M. L. Zelditch *et al.*, 2006 The brachymorph mouse and the developmental-genetic basis for canalization and morphological integration. *Evol. Dev.* 8: 61–73.
- Hallgrímsson, B., H. Jammniczky, N. M. Young, C. Rolian, T. E. Parsons *et al.*, 2009 Deciphering the palimpsest: studying the relationship between morphological integration and phenotypic covariation. *Evol. Biol.* 36: 355–376.
- Hayes, B. J., P. M. Visscher, and M. E. Goddard, 2009 Increased accuracy of artificial selection by using the realized relationship matrix. *Genet. Res.* 91: 47–60.
- Klingenberg, C. P., 1998 Heterochrony and allometry: the analysis of evolutionary change in ontogeny. *Biol. Rev. Camb. Philos. Soc.* 73: 79–123.
- Klingenberg, C. P., 2011 MorphoJ: an integrated software package for geometric morphometrics. *Mol. Ecol. Resour.* 11: 353–357.
- Klingenberg, C. P., 2009 Morphometric integration and modularity in configurations of landmarks: tools for evaluating a priori hypotheses. *Evol. Dev.* 11: 405–421.
- Klingenberg, C. P., 2013 Cranial integration and modularity: insights into evolution and development from morphometric data. *Hystrix* 24: 43–58.
- Klingenberg, C. P., and M. Zimmermann, 1992 Static, ontogenetic, and evolutionary allometry: a multivariate comparison in nine species of water striders. *Am. Nat.* 140: 601–620.
- Klingenberg, C. P., and L. J. Leamy, 2001 Quantitative genetics of geometric shape in the mouse mandible. *Evolution* 55: 2342–2352.
- Klingenberg, C., L. Leamy, E. Routman, and J. Cheverud, 2001 Genetic architecture of mandible shape in mice: effects of quantitative trait loci analyzed by geometric morphometrics. *Genetics* 157: 785–802.
- Laurie, C. C., K. F. Doheny, D. B. Mirel, E. W. Pugh, L. J. Bierut *et al.*, 2010 Quality control and quality assurance in genotypic data for genome-wide association studies. *Genet. Epidemiol.* 34: 591–602.
- Leamy, L., 1977 Genetic and environmental correlations of morphometric traits in random bred house mice. *Evolution* 31: 357–369.
- Li, M., J. B. Cole, M. Manyama, J. R. Larson, D. K. Liberton *et al.*, 2016 Rapid automated landmarking for morphometric analysis of three dimensional facial scans. *J. Anat.* (in press).
- Manfredi, C., R. Martina, G. B. Grossi, and M. Giuliani, 1997 Heritability of 39 orthodontic cephalometric parameters on MZ, DZ twins and MN-paired singletons. *Am. J. Orthod. Dentofacial Orthop.* 111: 44–51.
- Marcucio, R. S., N. M. Young, D. Hu, and B. Hallgrímsson, 2011 Mechanisms that underlie co-variation of the brain and face. *Genesis* 49: 177–189.
- Martínez-Abadías, N., M. Esparza, T. Sjøvold, R. González-José, M. Santos *et al.*, 2009a Heritability of human cranial dimensions: comparing the evolvability of different cranial regions. *J. Anat.* 214: 19–35.
- Martínez-Abadías, N., C. Paschetta, S. de Azevedo, M. Esparza, and R. González-José, 2009b Developmental and genetic constraints on neurocranial globularity: insights from analyses of deformed skulls and quantitative genetics. *Evol. Biol.* 36: 37–56.
- Martínez-Abadías, N., P. Mitteroecker, T. E. Parsons, M. Esparza, T. Sjøvold *et al.*, 2012 The developmental basis of quantitative craniofacial variation in humans and mice. *Evol. Biol.* 39: 554–567.
- Mitteroecker, P., and P. Gunz, 2009 Advances in geometric morphometrics. *Evol. Biol.* 36: 235–247.
- Ozsoy, U., B. M. Demirel, F. B. Yildirim, O. Tosun, and L. Sarikcioglu, 2009 Method selection in craniofacial measurements: advantages and disadvantages of 3D digitization method. *J. Craniomaxillofac. Surg.* 37: 285–290.
- Percival, C. J., D. K. Liberton, F. Pardo-Manuel De Villena, R. Spritz, R. Marcucio *et al.*, 2016 Genetics of murine craniofacial morphology: diallel analysis of the eight founders of the Collaborative Cross. *J. Anat.* 228(1): 96–112.
- Schlager, S., 2016 Morpho: Calculations and visualizations related to geometric morphometrics. R package version 2.4.1.1. <https://CRAN.R-project.org/package=Morpho>.
- Sperber, G. H., G. D. Guttman, and S. M. Sperber, 2001 *Craniofacial Development (Book for Windows & Macintosh)*. BC Decker Inc, Hamilton, ON.
- Visscher, P. M., G. Hemani, A. A. Vinkhuyzen, G.-B. Chen, S. H. Lee *et al.*, 2014 Statistical power to detect genetic (co)variance of complex traits using SNP data in unrelated samples. *PLoS Genet.* 10: e1004269.
- Wagner, G. P., M. Pavlicev, and J. M. Cheverud, 2007 The road to modularity. *Nat. Rev. Genet.* 8: 921–931.
- Yang, J., B. Benyamin, B. P. McEvoy, S. Gordon, A. K. Henders *et al.*, 2010 Common SNPs explain a large proportion of the heritability for human height. *Nat. Genet.* 42: 565–569.
- Yang, J., S. H. Lee, M. E. Goddard, and P. M. Visscher, 2011 GCTA: a tool for genome-wide complex trait analysis. *Am. J. Hum. Genet.* 88: 76–82.
- Zaitlen, N., P. Kraft, N. Patterson, B. Pasaniuc, G. Bhatia *et al.*, 2013 Using extended genealogy to estimate components of heritability for 23 quantitative and dichotomous traits. *PLoS Genet.* 9: e1003520.

Communicating editor: N. R. Wray